Influence of exciton-phonon coupling and strain on the anisotropic optical response of wurtzite AlN around the band edge

Georg Rossbach*
Institut für Physik, Technische Universität Ilmenau, PF100565, D-98684 Ilmenau, Germany

Martin Feneberg†
Institut für Experimentelle Physik, Otto-von-Guericke-Universität Magdeburg, Universitätsplatz 2, D-39106 Magdeburg, Germany

Marcus Röppischer, Christoph Werner, Norbert Esser, and Christoph Cobet
Leibniz-Institut für Analytische Wissenschaften, ISAS e.V., Albert-Einstein-Str. 9, D-12489 Berlin, Germany

Tobias Meisch and Klaus Thonke
Institut für Quantenmaterie/Gruppe Halbleiterphysik, Universität Ulm, D-89069 Ulm, Germany

Armin Dadgar, Jürgen Bläsing, and Alois Krost
Institut für Experimentelle Physik, Otto-von-Guericke-Universität Magdeburg, Universitätsplatz 2, D-39106 Magdeburg, Germany

Rüdiger Goldhahn
Institut für Experimentelle Physik, Otto-von-Guericke-Universität Magdeburg, Universitätsplatz 2, D-39106 Magdeburg, Germany and
Institut für Physik, Technische Universität Ilmenau, PF100565, D-98684 Ilmenau, Germany

(Received 27 January 2011; revised manuscript received 24 March 2011; published 4 May 2011)

The optical properties around the absorption edge of high-quality wurtzite *c*-plane AlN layers are investigated by spectroscopic ellipsometry focusing on the anisotropy of the optical response. The spectral dependence of dielectric function shows a strong contribution of exciton-phonon coupling superimposed to the exciton continuum. Crystal field splitting and spin-orbit coupling energies are found to be $\Delta_{cf} = -212$ meV and $\Delta_{so} = 16$ meV, respectively. These values are accessible because our data allow extraction of the transition energies of excitons with holes from all three highest valence bands. Energy positions are cross-checked by photoluminescence measurements. As the samples are grown on different substrates and exhibit varying biaxial strain determined by high resolution x-ray diffraction, we are also able to determine the deformation potentials $a - D_1 = -6.9$ eV, $a - D_2 = -15.2$ eV, $D_3 = 8.3$ eV, and $D_4 = -4.15$ eV for AlN.

DOI: 10.1103/PhysRevB.83.195202 PACS number(s): 78.40.Fy, 71.70.Ch, 71.70.Ej

I. INTRODUCTION

The binary wurtzite III-N semiconductors InN, GaN, and AlN and their ternary alloys are of high scientific and commercial interest due to the possibility of band-gap engineering between 0.675 and 6.015 eV at room temperature (RT) [1,2] while maintaining a direct optical band gap. The topmost valence band of AlN is of Γ_7 symmetry,[3–5] unlike the Γ_9 symmetry for InN[6,7] and GaN.[8] Consequently, in the case of AlN, for optical transitions different selection rules apply. This is just one of the very interesting aspects of wurtzite AlN. Despite intense research, even very fundamental parameters of the binary AlN are still under debate such as the excitonic transition energies for strain-free material,[5] the binding energies of excitons,[2,9,10] or the deformation potentials. Investigations are hampered by problematic crystal growth and experimental difficulties arising from the ultraviolet spectral region at around 6 eV, where the fundamental band-edge of wurtzite AlN is found. However, further progress in understanding ternary nitrides, i.e., AlInN and AlGaN, are dependent on a reliable knowledge of basic parameters of AlN. It is therefore very demanding to study basic parameters of AlN to give future research and development a better fundament.

Due to the hexagonal lattice structure of wurtzite crystals, all optical properties of AlN show a pronounced anisotropy with respect to the optical axis (**c** axis or [0001]). It is described by the ordinary ($\bar{\varepsilon}_o = \varepsilon_{1,o} + i\varepsilon_{2,o}$) and extraordinary ($\bar{\varepsilon}_e = \varepsilon_{1,e} + i\varepsilon_{2,e}$) dielectric functions (DFs) corresponding to electric field (**E**) polarized perpendicular and parallel to the optical axis, respectively. In the vicinity of the band gap this is caused by the ordering of the three valence bands around the Γ point of the Brillouin zone and their symmetries, resulting in corresponding optical oscillator strengths for different polarizations of the electric field: $\mathbf{E}\perp\mathbf{c}$ and $\mathbf{E}\parallel\mathbf{c}$. The sequence of the valence bands in order of decreasing energy is Γ_7, Γ_9, and Γ_7 with a large distance between the topmost Γ_7 and the other two valence bands due to the large negative crystal field energy Δ_{cf}. The corresponding transitions from the conduction band (which has Γ_7 symmetry as well) to the valence bands are labeled in increasing absolute energy as *A*, *B*, and *C* in the following. The *B* transition is allowed only for $\mathbf{E}\perp\mathbf{c}$ and thus only observable in $\bar{\varepsilon}_o$. Transitions *A* and *C* are allowed for both $\mathbf{E}\perp\mathbf{c}$ and $\mathbf{E}\parallel\mathbf{c}$. However, the *A* transition in AlN has an oscillator strength close to zero for $\mathbf{E}\perp\mathbf{c}$, i.e., it appears only weak in $\bar{\varepsilon}_o$ but strong in $\bar{\varepsilon}_e$. Transition *C* exhibits the opposite polarization behavior.

Reflection studies on (0001) oriented AlN under normal incidence of light ($\mathbf{E}\perp\mathbf{c}$) do not allow resolution of

transition A. This problem can be solved by applying spectroscopic ellipsometry (SE) as demonstrated recently. The high angle of incidence allows us to probe both real and imaginary parts of ε_e, while ε_o is detectable also for a low angle of incidence.[11,12]

In this work the analysis of the anisotropic response of the excitonic band edge of wurtzite AlN is addressed. Low-temperature SE studies of the (0001) films lead to considerably sharper features in $\bar{\varepsilon}_o$ and $\bar{\varepsilon}_e$ compared to previous investigations. We demonstrate that exciton-phonon coupling (EPC) has a strong impact on the spectral dependence of the DF around the band edge being completely disregarded so far. Therefore, the model for describing the DF has to take into account the EPCs in addition to the free excitonic resonances and the exciton continuum described by Elliot's model.[13] Thus, the current work exceeds the common approach to describe excitonic resonances by simple Lorentz oscillators (mostly from reflectivity spectra[4,5,14,15]) and increases the reliability of experimental transition energies.

Low-temperature data are compared to emission spectra from the same samples further supporting the model used. In temperature-dependent spectra, the exciton-phonon coupling as well as excitons can be monitored up to room temperature. Finally, we are able to derive values for fundamental parameters of AlN like crystal field splitting energy, spin-orbit coupling, and deformation potentials as our set of six samples spans a wide range of strain states from biaxially tensile to compressive.

II. SAMPLES

To investigate optical properties as a function of stress, undoped AlN layers were grown on sapphire(0001), silicon(111), and silicon-carbide [6H-SiC(0001)] substrates, resulting in different biaxial in-plane strain because of thermal and lattice mismatch. Samples on sapphire (Sa1-3) and silicon (Si1-2) were grown by metal-organic chemical vapor deposition in a Thomas Swan $6 \times 2''$ showerhead reactor using trimethylaluminum (TMAl) and ammonia as precursors. Growth was started by a low-temperature nucleation layer (700° C) using a short Al predeposition before ammonia supply. Applied precursor flux (standard cubic centimeter, sccm) and substrate temperature for the subsequently deposited about 300-nm-thick high-temperature layers are shown in Table I. Complementary information can be found elsewere.[11,16] Note that sample S2 from Ref. 11 is excluded from the present study, because we suspect a small fraction (about 0.5%) of gallium being incorporated in this layer, falsifying its results.

In contrast, sample Sc on SiC was grown by plasma-assisted molecular beam epitaxy: substrate temperature and nitrogen flux were kept constant at 830° C and 1 sccm during the process, respectively. The deposited layer has a thickness of about 700 nm. After growth, the layers were characterized by high resolution x-ray diffraction (XRD) proving pure *c*-plane orientation. The lattice parameters are summarized in Table I.

TABLE I. Growth conditions, lattice parameters, and strain states of all samples.

Substrate	Sample	NH_3 (sccm)	TMAl (sccm)	T_{Growth} (°C)	c (Å)	ϵ_{zz} (10^{-4})
Silicon	Si1	500	180	1300	4.9692	−23.5
	Si2	500	60	1150	4.9694	−23.1
Sapphire	Sa1	250	180	1300	4.9810	0.2
	Sa2	500	180	1300	4.9820	2.2
	Sa3	1000	180	1300	4.9826	3.4
6H-SiC	Sc	1	–	830	4.985	8.3

III. EXPERIMENTAL

Spectroscopic ellipsometry has proven to be a powerful tool to study optical properties of thin film layers. Measurements in the photon energy range up to 6.4 eV using variable angles of incidence were carried out with a commercial J. A. Woollam ellipsometer. Complementary SE studies in the vacuum-ultraviolet range above 5 eV in steps of about 1 meV were performed by a rotating-analyzer ellipsometer located at the synchrotron radiation source BESSY II in Berlin, described in detail in Ref. 17. Here, the angle of incidence is fixed to 67.5°, while the use of a helium-flow cryostat opens the possibility to perform measurements at temperatures from room temperature down to 10 K. Low-temperature data are only available for samples Si1, Sa3, and Sc.

All layers within this study have *c*-plane (or [0001]) orientation: Under normal incidence, the electric field of light (**E**) is completely polarized perpendicular to the optical axis. Hence, the optical response (reflectivity) exclusively depends on the ordinary component ε_o of the dielectric function. Considering an oblique incidence, components of light polarized parallel and perpendicularly to the plane of incidence experience different parts of the DF. For the perpendicularly polarized component identical conclusions are valid as previously mentioned for normal incidence. The parallel component is always partly polarized parallel to the optical axis: the influence of the extraordinary DF ε_e increases with higher incidence angle. Spectroscopic ellipsometry preferably operating around the Brewster angle is therefore partially sensitive to ε_e, demonstrated for the transparent region of GaN and AlN by Shokhovets *et al.*[18] and for the region around the band edge by Refs. 11 and 12. In the case of AlN the pronounced dichroism in the vicinity of the absorption edge—the band gap of ε_e is located about 200 meV below the gap of ε_o—leads to an even higher sensitivity in this energy range.[11]

IV. RESULTS AND DISCUSSION

A. SE data analysis

Experimental data were analyzed by a previous published method[19] based on a multi-layer model, taking into account interface and surface roughness (typical layer thickness between 2.5 and 3 nm as a mixture of the adjacent materials) and the optical anisotropy of AlN.[11] In *c*-plane layers, in the vicinity of the band edge, the pronounced dichroism of AlN leads to an increased sensitivity of ellipsometric measurements (carried out under high angles of incidence) to ε_e. Nevertheless, compared to ε_o the impact is still weak, allowing the use of a parametric modeling for ε_e. Here, the parametric model

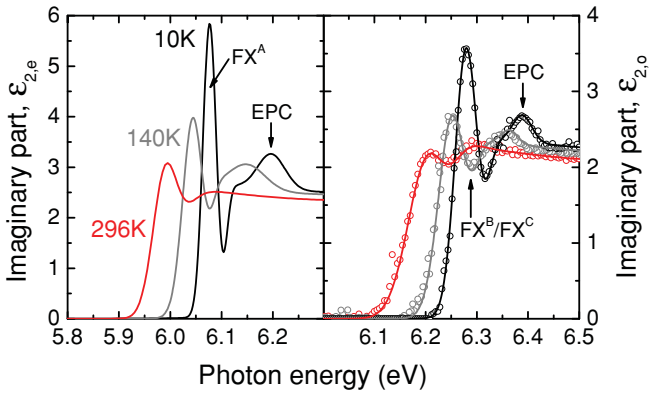

FIG. 1. (Color online) Imaginary part of the extraordinary (left) and ordinary (right) dielectric function (DF) of sample Sa3 for temperatures of 10 K (black), 140 K (gray), and 296 K (red). The point-by-point fitted DF is shown as open circles while the continuous lines represents the DF as described by the model (see text).

introduced by Johs *et al.* was applied, in which high-energy critical points of the band structure are represented by so-called Psemi oscillators, engineered by connected spline functions.[20,21] Since no experimental results of ε_e above the band edge of AlN are published so far and sensitivity in this range is negligible for *c*-plane films, spectral characteristics of ε_e above the band gap are based on *first-principles* calculations and were kept constant for all samples.[22] The accuracy of this approach has been proven in Ref. 11. The band-edge region has been modeled by the line shape described in detail below, i.e., the excitonic resonances, the exciton continuum, and EPC were taken into account.

In contrast, the sensitivity to ε_o is high over the whole spectral range. Here, no assumption was made concerning the shape of the DF. Keeping the layer model and the influence of the ε_e, every pair of $\varepsilon_{1,o}$ and $\varepsilon_{2,o}$ at photon energy E was fitted separately to the experimental data, resulting in a so-called point-by-point DF (PbP-DF). Figure 1 shows, as a typical example, the imaginary parts of ε_e and ε_o of sample Sa3 at three temperatures. The parametric model DF is represented by continuous lines, while the PbP DF is drawn as open circles. Agreement between both data sets is very good.

In the sense of a detailed analysis, the imaginary part of ε_o was further investigated. It consists of contributions from two valence bands: Γ_9 and Γ_7, transitions B and C, respectively. These were treated following Elliot's classical theory[13]:

$$\varepsilon_{2,o}^{\mathrm{El}}(E) = \sum_{\mathrm{vb}=\Gamma_9^v,\Gamma_{7-}^v} \varepsilon_2^{X,\mathrm{vb}}(E) + \varepsilon_2^{\mathrm{BB,vb}}(E), \qquad (1)$$

where, in agreement with the large negative crystal field leading to almost identical oscillator strengths, the only difference between both bands is the energetic position of the transition (expressed by $\bar{E}_{BC}$).

It is known from other polar materials[23] that in addition to the excitonic (X) and the band-to-band (BB) a third contribution comes into play caused by Fröhlich interaction: Coulomb interaction between free carriers and the electric field induced by longitudinal-optical (LO) phonons. The corresponding bound states lead to a characteristic increase of absorption above the free-exciton resonance. Liang and Yoffe observed this EPC for the first time, carrying out transmission measurements on ZnO single crystals.[24] With respect to the spectra obtained especially at low temperatures, EPCs have to be taken into account to reach a satisfactory modeling. We therefore followed the approach of Shokhovets *et al.*,[23] who investigated EPCs in GaN and ZnO complementing Elliot's theory by adding the m^{th} phonon replica energetically shifted by E_{LO}:

$$\varepsilon_{2,o}(E) = \varepsilon_{2,o}^{\mathrm{El}}(E) + \sum_{vb=\Gamma_9^v,\Gamma_{7-}^v} f^0 \sum_{m=1}^{N_m} b^{m-1} \varepsilon_2^{X,vb}(E - m E_{\mathrm{LO}}). \qquad (2)$$

Excited states of the excitons are taken into account in a similar way:

$$\varepsilon_2^{X,vb} = \frac{f^X}{(\hbar\omega)^2} \sum_n \gamma^{-1} n^{-3} \exp\left[-\frac{(\hbar\omega - E_n)^2}{\gamma^2} \right]. \qquad (3)$$

Parameters in Eqs. (1)–(3) to be modeled are the energy positions of band-to-band absorption E_G, binding energy of the excitons E_{bX}, their broadening γ, and the phonon energy E_{LO}. n is the exciton state with $E_n = E_G - E_{bX}/n^2$. Oscillator strengths of excitons and band-to-band contributions are expressed by f^X and f^{BB}, respectively. The strength of the EPC contribution can be abbreviated as $f^{\mathrm{EPC}} = f^0 \sum_{m=1}^{N_m} b^{m-1}$

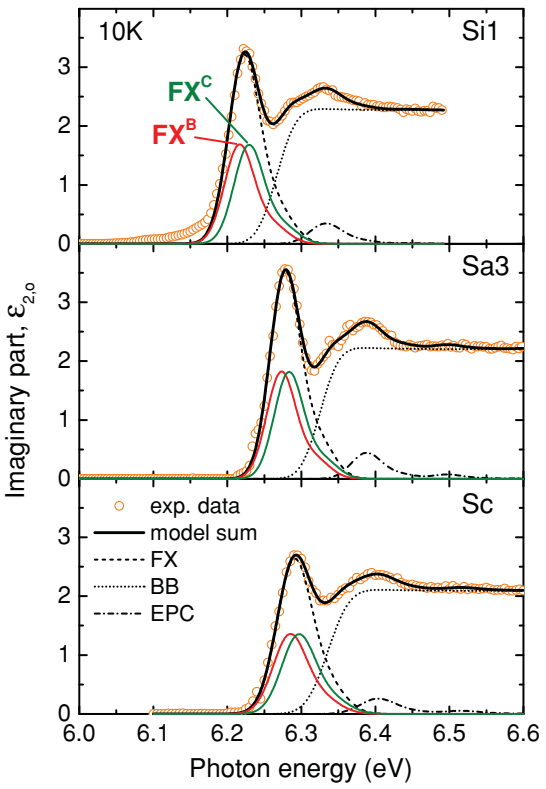

FIG. 2. (Color online) Imaginary part of the ordinary dielectric function at $T = 10$ K of three samples grown on different substrates. The open circles represent point-by-point data, continuous lines the model (see text). The contributions to the model are shown separately, where FX^B (FX^C) labels the contributions from the free excitons, BB is the band-to-band absorption, and EPC the electron-phonon contribution.

with b being forced to be less than unity. In Fig. 2, low temperature $\varepsilon_{2,o}$ of samples grown on different substrates are shown. The parametric model, represented by the continuous line, agrees very well with the PbP DF (open circles). Furthermore, in Fig. 2, different contributions to the parametric model of $\varepsilon_{2,o}$ are shown separately. These are namely the band-to-band transitions (BB), two free excitonic resonances (the lower in energy is FX^B, the higher one FX^C), and the exciton-phonon contribution labeled EPC. Note that no reasonable agreement without the EPC could be found. The two exciton transitions in $\varepsilon_{2,o}$ are fitted with variable energy distance for each sample (the values vary between 10 and 13 meV). By doing so, reasonable exciton binding energies of around 58 meV are obtained (see Table III), in contrast to a much-too-low binding energy of around 42 meV when taking only one exciton into account.

A comparable model for the DF describing EPC was published by Müller *et al.*[25] We compared it with our model for several DFs of different samples and found no characteristic differences in any fitting result: Energy positions coincide within 1 meV, and oscillator strengths differ less than 1%. This agreement shows independently the high reliability of our fitting procedure.

The excellent agreement for $\varepsilon_{2,o}$ between the experimental PbP data and the parametric model DF (excitons and exciton-phonon coupling) provides a further proof of the accuracy of the model DF. It was therefore used for determining $\varepsilon_{2,e}$ yielding, in particular, the free exciton energy $E(FX^A)$. The binding energy amounts here to around 58 meV as well (compare to the calculated values of 72.5 and[9] 51 meV[10] and the experimental value of 55 meV[2]).

B. Low-temperature transition energies

Three representative samples spanning the whole investigated strain range were investigated by SE at 10 K (Fig. 2). All samples show the same contributions in $\varepsilon_{2,o}$ including EPC. However, dependent on the strain situation of the samples governed by underlying substrate, we find the transitions at different energy positions. Fitting results of these three samples are summarized in Table II.

To underline our analysis further and increase the reliability of our data, we compare now values obtained by SE with photoluminescence (PL) peak positions from the same layers (Fig. 3). Note that we find a PL signal from all layers except sample Sc. The near-band-edge PL spectra of all samples consists of a single broad peak with shifting energy position.

TABLE II. Energy positions as extracted from $\varepsilon_{2,o}$ and PL at low temperature ($T = 10$ K).

Sample	E(PL) (eV)	$E(FX^A)$ (eV)	$E(FX^B)$ (eV)	$E(FX^C)$ (eV)	E_{bX} (meV)	ΔE_{loc} (meV)
Si1	5.936	5.958	6.216	6.229	57	22
Si2	5.951	–	–	–	–	–
Sa1	6.040	–	–	–	–	–
Sa2	6.044	–	–	–	–	–
Sa3	6.057	6.074	6.273	6.283	58	17
Sc	–	6.109	6.285	6.295	57	–

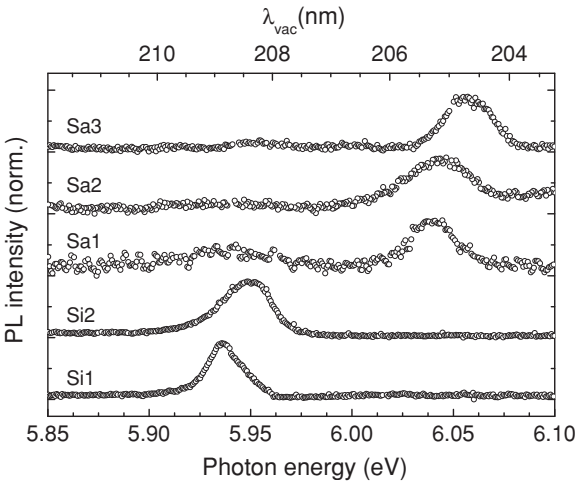

FIG. 3. Photoluminescence (PL) spectra recorded at 10 K of the samples Sa1-3 and Si1-2 showing the near-band-gap energy region. Peak positions of PL spectra show excellent agreement to free exciton energies based on spectroscopic ellipsometry (see text).

As we have low-temperature SE data from three layers including sample Sc, we have the possibility of comparing energy values obtained by PL and SE from two layers, namely Si1 and Sa3. For both samples, the PL signal is peaking at lower energy than is the value of FX^A. This is expected, as emission should be dominated by (donor) bound exciton complexes, while SE yields the energy of free excitonic transitions. The difference between both values is identical to the exciton localization energy that is a characteristic value of the donor species involved in the emission process. Interestingly, sample Sa3 shows a localization energy of 17 meV while Si1 has 22 meV (summarized as ΔE_{loc} in Table II). The value of 22 meV is identical to the localization energy reported earlier for that of the exciton bound to the neutral donor silicon.[2,15,26–28] This allows the conclusion that the dominant donor in sample Si1 is silicon—a reasonable assignment for heteroepitaxy on silicon. The dominating donor in sample Sa3 with 17 meV localization energy is close to a different—but yet not identified—shallow donor in AlN having about 13 meV localization energy in earlier works.[2,14,26]

C. Temperature-dependent data

Figure 4 shows ordinary DFs of sample Sc recorded between 10 K and RT. Obviously, the EPC contributions (marked by arrows) are observable up to RT and cannot be disregarded in the data analysis. For each temperature, all model parameters were extracted separately. The energy position of the free exciton (FX^B) in $\varepsilon_{2,o}$ can be described using the equation introduced by Viña *et al.*[29]:

$$E(T) = E(0) - \frac{2\alpha}{\exp(\Theta/T) - 1}, \tag{4}$$

where the parameters which describe the behavior best are $E(0) = 6.285$ eV, $\Theta = 447$ K, and $\alpha = 144$ meV (Fig. 4). These values agree well with previously published results for FX^A.[2,15,30] The energy shift due the temperature increase between 10 K and 295 K amounts to ≈80 meV. This agrees well with the temperature-dependent energy shift found in

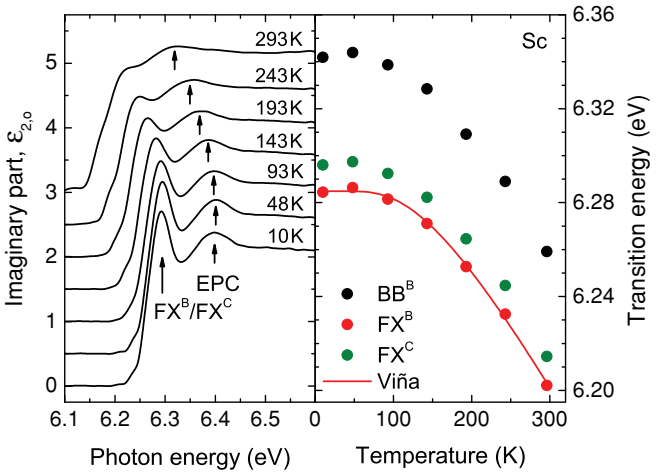

FIG. 4. (Color online) Sample Sc. (Left) Imaginary part of the PbP ordinary DF around the band gap as a function of temperature. Spectra were vertically shifted by 0.5 for clarity and (right) energy positions from $\varepsilon_{2,o}$ as a function of temperature. Shown are the extracted energy positions for FX^B and FX^C, as well as the peak position of the EPC. The continuous line is a model fit of the dependence.

samples Sa3 and Si1, where only selected temperatures have been chosen for SE spectra (Fig. 1). The absolute energy shift of FX^B measured by SE was therefore taken over for FX^A to obtain the values for $E(FX^A)$ at $T = 10$ K as shown in Table II.

At room temperature, results from all samples are available where the DF model was fitted to PbP data. This yields the parameters as described with very high accuracy. By comparing the results obtained from AlN layers grown on different substrates, we find differences especially in the energy position of the excitons (Fig. 2). The most important parameters extracted for the different samples at room temperature are summarized in Table III.

The LO phonon energy is derived from the position of the EPC and is in average of our seven samples at room temperature 110.4 meV in perfect agreement with the reported LO-phonon energy determined by different experimental techniques.[31]

TABLE III. Energy positions extracted from the DFs for all samples at room temperature. The values obtained by our analysis for unstrained material are shown additionally labeled strain-free.

Sample	$E(FX^A)$ (eV)	$E(FX^B)$ (eV)	$E(FX^C)$ (eV)	E_{bX} (meV)	E_{LO} (meV)
Si1	5.873	6.131	6.143	59	110
Si2	5.867	6.125	6.136	58	108
Sa1	5.964	6.175	6.185	59	102
Sa2	5.978	6.191	6.202	56	113
Sa3	5.989	6.188	6.199	59	110
Sc	6.026	6.202	6.215	57	112
Strain-free	5.974	6.181	6.192	–	–

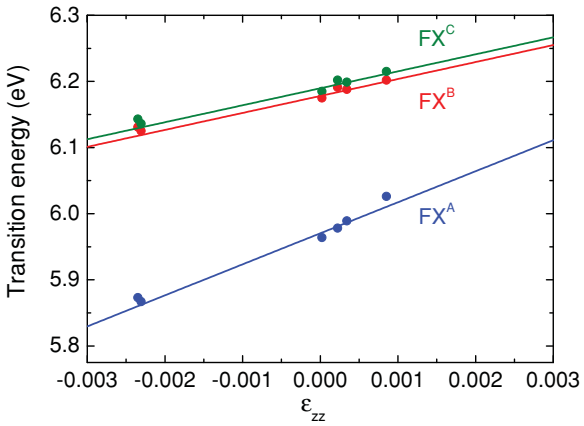

FIG. 5. (Color online) Energy positions of free exciton transitions at room temperature as a function of ϵ_{zz} (symbols) and corresponding calculations using **kp** theory (continuous lines).

D. Strain analysis

Our samples cover different biaxial strain situations from compressive to tensile (see Table I). Therefore, we are able to analyze the strain dependence of all three excitonic transitions. To determine the strain, experimental lattice constants are compared to the value for relaxed material reported by Paszkowicz and coworkers[32] of $c = 4.980\,89$ Å. First, we have a look at the low-temperature PL data (Fig. 3). Sample Sa1 has a PL signal peaking at 6.040 eV. The c-lattice constant of this sample is very close to that of strain-free AlN (Table I) and we note that the transition energy is in good agreement with the value of 6.0414 eV for FX^A reported in Ref. 26 for homoepitaxially grown AlN.

Energy positions (room-temperature SE data) of excitonic contributions are then plotted as a function of out-of-plane strain ϵ_{zz} (Fig. 5), which allows investigation of deformation potentials. Therefore, the band structure was modeled using quasicubic approximation in **kp** theory. The energy positions of the valence bands are described by the approach introduced by Chuang and Chang[33] following earlier work of Bir and Pikus.[34] At the Γ point of the Brillouin zone, the energies are

$$E_c = \Delta_{\rm cf} + \frac{\Delta_{\rm so}}{3} + E_{gB} + P_{c\epsilon} - E_{bX}$$

$$E_{vA/C} = \frac{\Delta_{\rm cf} - \frac{\Delta_{\rm so}}{3} + \Theta_\epsilon}{2} + \lambda_\epsilon \pm \sqrt{\left(\frac{\Delta_{\rm cf} - \frac{\Delta_{\rm so}}{3} + \Theta_\epsilon}{2}\right)^2 + \frac{2}{9}\Delta_{\rm so}^2}$$

$$E_{vB} = \Delta_{\rm cf} + \frac{\Delta_{\rm so}}{3} + \Theta_\epsilon + \lambda_\epsilon,$$

where E_c is the strain-dependent conduction band energy already corrected for the binding energy of excitons (E_{bX}) and E_{vj} ($j = A, B, C$) are the valence band energies. Using the identities

$$\Theta_\epsilon = D_3\epsilon_{zz} + D_4(\epsilon_{xx} + \epsilon_{yy})$$
$$\lambda_\epsilon = D_1\epsilon_{zz} + D_2(\epsilon_{xx} + \epsilon_{yy})$$
$$P_{c\epsilon} = a_{||}\epsilon_{zz} + a_\perp(\epsilon_{xx} + \epsilon_{yy}),$$

TABLE IV. Crystal field splitting Δ_{cf}, spin-orbit splitting Δ_{so}, and deformation potentials as reported in the literature in comparison to our results. Values in brackets are used as input parameters in the respective references. In Ref. 39 direct values for D_1 and D_2 are reported, these would yield in comparison with our results consistently $a = (-23.6 \pm 0.5)$eV.

	Δ_{cf} (meV)	Δ_{so} (meV)	$a - D_1$ (eV)	$a - D_2$ (eV)	D_3 (eV)	D_4 (eV)
This study	-212 ± 2	16 ± 3	-6.9 ± 0.6	-15.2 ± 0.3	8.3 ± 0.3	-4.15 ± 0.2
Ref. 38	-275.8	21.8				
Ref. 35	-152.4	18.9	-8.4	-15.6	8.19	-4.1
Ref. 15	-237	(20)				
Ref. 4	-230	(20)				
Ref. 40	-244		-3.39	-11.81	9.42	-4.02
Ref. 39	-176		$a + 17.1$	$a + 7.92$	8.84	-3.92

we have the valence and conduction band energies as a function of in-plane and out-of-plane strain multiplied by the deformation potentials D_i ($i = 1$–4). In cubic approximation, the set of valence band deformation parameters can be simplified to only two independent values

$$D_1 - D_2 = -D_3 = 2D_4. \tag{5}$$

For the deformation potential of the conduction band, the two deformation potentials $a_{||}$ and $a_{\perp}$ are required. For simplicity, we assume both to be equal $a = a_{\perp} = a_{||}$. One further assumption, already made when fitting the dielectric functions, is that all three exciton binding energies $E_{bX} \approx 58$ meV (see Table III) in AlN are equal and not dependent on strain. This is a reasonable assumption in the investigated strain regime.[35]

By knowledge of elastic constants which link the different strain values in our equations via

$$\epsilon_{xx} = \epsilon_{yy}$$
$$\epsilon_{xx} = -\frac{C_{33}}{2C_{13}}\epsilon_{zz},$$

the energy distances of the different valence bands can now be used to calculate Δ_{cf}, Δ_{so}, $a - D_1$, and $a - D_2$. From these parameters one can compute in cubic approximation D_3 and D_4. For the elastic constants we use $C_{33} = 373$ GPa and $C_{13} = 108$ GPa.[36]

From the energy differences at $\epsilon_{zz} = 0$ between FX^B and FX^A or FX^C, respectively, the crystal field energy and the spin-orbit splitting are obtained. Only the differences $\bar{E}_{AB}$ and $\bar{E}_{BC}$ of the absolute transition energies play a role and are used in

$$\Delta_{cf} = \tfrac{1}{2}[\bar{E}_{BC} - \bar{E}_{AB} - \sqrt{(\bar{E}_{AB} + \bar{E}_{BC})^2 + 2\bar{E}_{AB}\bar{E}_{BC}}], \tag{6}$$

while Δ_{so} can be expressed as

$$\Delta_{so} = \tfrac{1}{2}[\bar{E}_{BC} - \bar{E}_{AB} + \sqrt{(\bar{E}_{AB} + \bar{E}_{BC})^2 + 2\bar{E}_{AB}\bar{E}_{BC}}]. \tag{7}$$

After plotting our experimental exciton transition energies as a function of ϵ_{zz} (Fig. 5), we fitted for each exciton a linear curve that is justified because we are far away from the anticrossing of the valence bands that happens at large positive ϵ_{zz}.[35] From these fitted lines, $\bar{E}_{BA}$ and $\bar{E}_{BC}$ are calculated and yield $\Delta_{cf} = -212$ meV and $\Delta_{so} = 16$ meV.

The deformation potentials are obtained from the slopes of the exciton transitions as a function of strain, similarly to the approach shown in Ref. 37. These relations are given as

$$E_c - E_{vA} \propto \left[(a - D_1) - \frac{C_{33}}{C_{13}}(a - D_2)\right]\epsilon_{zz}$$
$$E_c - E_{vB} \propto \left[(a - D_1 - D_3) - \frac{C_{33}}{C_{13}}(a - D_2 - D_4)\right]\epsilon_{zz}$$
$$E_c - E_{vC} \propto \left[(a - D_1 - D_3) - \frac{C_{33}}{C_{13}}(a - D_2 - D_4)\right]\epsilon_{zz},$$

where the slopes are found in square brackets. The slopes of the B and C excitons are expected to be equal and are indeed found to be identical within a relative error of less than 2×10^{-3}. The deformation potentials are $a - D_1 = -6.9$ eV, $a - D_2 = -15.2$ eV and thus $D_3 = 8.3$ eV and $D_4 = -4.15$ eV in the cubic approximation. These findings compare favorably to previously reported values from both theory and experiment and are summarized in Table IV.

The FX^A transition energy at $\epsilon_{zz} = 0$ is evaluated to be 5.974 eV, close to the corresponding transitions of our least-strained samples Sa1 and Sa2 (Table III). The corresponding energies for FX^B and FX^C are 6.181 and 6.192 eV, respectively.

V. SUMMARY

We experimentally evaluated transition energies of excitons with holes from the three highest valence bands in AlN layers based on absorption and emission studies. These layers were grown heteroepitaxially on different substrates and exhibit strain from biaxially compressive to tensile. By comparing strain state and exciton positions, we derive a crystal field splitting of $\Delta_{cf} = -212$ meV, a spin-orbit splitting of $\Delta_{so} = 16$ meV, and the deformation potentials $a - D_1 = -6.9$ eV, $a - D_2 = -15.2$ eV, $D_3 = 8.3$ eV, and $D_4 = -4.15$ eV. The influence of exciton-phonon coupling on the absorption characteristics, dominated by LO phonons, could be shown conclusively.

ACKNOWLEDGMENTS

We thank Azzurro Semiconductors, Magdeburg, Germany, and the Paul Drude-Institut, Berlin, Germany, for the growth of samples. This work was supported by the BMBF (05ES3XBA/5), the *Thüringer Kultusministerium* (EFRE, B715-08015), and the *Deutsche Forschungsgemeinschaft* (KR2228-3). We gratefully acknowledge funding of part of this work by the Deutsche Forschungsgemeinschaft within the framework of collaborative research center 787. We gratefully acknowledge support by the synchrotron radiation source BESSY II of the Helmholtz-Zentrum Berlin (HZB).

---

*Now at Institute of Condensed Matter Physics, Ecole Polytechnique Fédérale de Lausanne (EPFL), CH-1015 Lausanne, Switzerland.

†Corresponding author: martin.feneberg@ovgu.de

[1] P. Schley, R. Goldhahn, G. Gobsch, M. Feneberg, K. Thonke, X. Wang, and A. Yoshikawa, Phys. Status Solidi B **246**, 1177 (2009).

[2] M. Feneberg, R. A. R. Leute, B. Neuschl, K. Thonke, and M. Bickermann, Phys. Rev. B **82**, 075208 (2010).

[3] S.-H. Wei and A. Zunger, Appl. Phys. Lett. **69**, 2719 (1996).

[4] L. Chen *et al.*, Appl. Phys. Lett. **85**, 4334 (2004).

[5] E. Silveira, J. A. Freitas, O. J. Glembocki, G. A. Slack, and L. J. Schowalter, Phys. Rev. B **71**, 041201(R) (2005).

[6] K. Wang, T. Yamaguchi, A. Takeda, T. Kimura, K. Kawashima, T. Araki, and Y. Nanishi, Phys. Status Solidi A **207**, 1356 (2010).

[7] P. Schley, J. Räthel, E. Sakalauskas, G. Gobsch, M. Wieneke, J. Bläsing, A. Krost, G. Koblmüller, J. S. Speck, and R. Goldhahn, Phys. Status Solidi A **207**, 1062 (2010).

[8] P. Misra, O. Brandt, H. T. Grahn, H. Teisseyre, M. Siekacz, C. Skierbiszewski, and B. Łucznik, Appl. Phys. Lett. **91**, 141903 (2007).

[9] B. Gil, Phys. Rev. B **81**, 205201 (2010).

[10] B. Gil, B. Guizal, D. Felbacq, and G. Bouchitté, Eur. Phys. J. Appl. Phys. **53**, 20303 (2011).

[11] G. Rossbach, M. Röppischer, P. Schley, G. Gobsch, C. Werner, C. Cobet, N. Esser, A. Dadgar, M. Wieneke, A. Krost, and R. Goldhahn, Phys. Status Solidi B **247**, 1679 (2010).

[12] W. Jiang, W. Lin, S. Li, J. Chen, and J. Kang, Opt. Mater. **32**, 891 (2010).

[13] R. Elliot, Phys. Rev. **108**, 1384 (1957).

[14] T. Onuma, T. Shibata, K. Kosaka, K. Asai, S. Sumiya, M. Tanaka, T. Sota, A. Uedono, and S. F. Chichibu, J. Appl. Phys. **105**, 023529 (2009).

[15] G. M. Prinz, A. Ladenburger, M. Schirra, M. Feneberg, K. Thonke, R. Sauer, Y. Taniyasu, M. Kasu, and T. Makimoto, J. Appl. Phys. **101**, 023511 (2007).

[16] A. Dadgar, A. Krost, J. Christen, B. Bastek, F. Bertram, A. Krtschil, T. Hempel, J. Bläsing, U. Haboeck, and A. Hoffmann, J. Cryst. Growth **207**, 306 (2006).

[17] C. Cobet, R. Goldhahn, W. Richter, and N. Esser, Phys. Status Solidi B **246**, 1440 (2009).

[18] S. Shokhovets, R. Goldhahn, G. Gobsch, S. Piekh, R. Lantier, A. Rizzi, V. Lebedev, and W. Richter, J. Appl. Phys. **94**, 307 (2003).

[19] R. Goldhahn, Acta Phys. Polonica A **104**, 123 (2003).

[20] B. Johs, C. M. Herzinger, J. H. Dinan, A. Cornfeld, and J. D. Benson, Thin Solid Films **313**, 137 (1998).

[21] C. M. Herzinger and B. D. Johs, U.S.-Patent No. 5796983 (1998).

[22] L. X. Benedict, T. Wethkamp, K. Wilmers, C. Cobet, N. Esser, E. L. Shirley, W. Richter, and M. Cardona, Solid State Commun. **112**, 129 (1999).

[23] S. Shokhovets, O. Ambacher, B. K. Meyer, and G. Gobsch, Phys. Rev. B **78**, 035207 (2008).

[24] Liang and Yoffe, Phys. Rev. Lett. **20**, 59 (1968).

[25] A. Müller, G. Benndorf, S. Heitsch, C. Sturm, and M. Grundmann, Solid State Commun. **148**, 570 (2008).

[26] M. Feneberg, B. Neuschl, K. Thonke, R. Collazo, A. Rice, Z. Sitar, R. Dalmau, J. Xie, S. Mita, and R. Goldhahn, Phys. Status Solidi A, accepted (2011).

[27] G. M. Prinz, M. Feneberg, M. Schirra, R. Sauer, K. Thonke, S. B. Thapa, and F. Scholz, Phys. Stat. Sol. RRL **2**, 215 (2008).

[28] K. B. Nam, M. L. Nakarmi, J. Li, J. Y. Lin, and H. X. Jiang, Appl. Phys. Lett. **83**, 2787 (2003).

[29] L. Viña, S. Logothetidis, and M. Cardona, Phys. Rev. B **30**, 1979 (1984).

[30] H. Murotani, T. Kuronaka, Y. Yamada, T. Taguchi, N. Okada, and H. Amano, J. Appl. Phys. **105**, 083533 (2009).

[31] J. G. Tischler and J. A. Freitas, Appl. Phys. Lett. **85**, 1943 (2004).

[32] W. Paszkowicz, S. Podsiado, and R. Minikayev, J. Alloys Compounds **382**, 100 (2004).

[33] S. L. Chuang and C. S. Chang, Phys. Rev. B **54**, 2491 (1996).

[34] G. L. Bir and G. E. Pikus, *Symmetry and Strain Induced Effects in Semiconductors* (Wiley, New York, 1974).

[35] H. Ikeda *et al.*, J. Appl. Phys. **102**, 123707 (2007).

[36] I. Vurgaftman and J. R. Meyer, J. Appl. Phys. **94**, 3675 (2003).

[37] H. Y. Peng, M. D. McCluskey, Y. M. Gupta, M. Kneissl, and N. M. Johnson, Phys. Rev. B **71**, 115207 (2005).

[38] L. C. d. Carvalho, A. Schleife, F. Fuchs, and F. Bechstedt, Appl. Phys. Lett. **97**, 232101 (2010).

[39] K. Shimada, T. Sota, and K. Suzuki, J. Appl. Phys. **84**, 4951 (1998).

[40] J. M. Wagner and F. Bechstedt, Phys. Rev. B **66**, 115202 (2002).